Structural Study on Iron Oxide Nanoparticles Prepared by Sol-Gel Method

Akiba Fexy J D H

Abstract—Fine nanosized metal oxide namely, iron oxide (α-Fe_2O_3) has been synthesized by sol-gel method using Ferric Chloride as the starting precursor. X-ray diffraction (XRD) study has been conducted to identify the polymorph of the prepared iron oxide nanoparticles. From the study it was observed that the prepared nanoparticles exhibited rhombohedral α-Fe_2O_3 phase without any other phases magnetite (Fe_3O_4) or a mixture of magnetite (Fe_3O_4) and maghemite (γ-Fe_2O_3). All the structural parameters such as lattice constants, unit cell volume, density, crystalline size, micro strain, dislocation density, texture co-efficient were calculated from the XRD results.

Index Term — nanoparticle; Fe_2O_3; sol-gel; XRD; hematite; rhombohedral;maghemite

1 Introduction

Transition metal oxides have many applications as catalysts, sensors, superconductors, and many bio-medical applications. Metal oxides constitute an important class of materials that are involved in environmental science, electrochemistry, biology, chemical sensors, magnetism, and other fields. One of the most important applications is bio-medical applications. Iron oxide belongs to the most abundant minerals and occurs with a large variety of stoichiometries, structures, and properties. Iron oxide exists in three forms in nature: magnetite (Fe3O4), maghemite (γ-Fe2O3), and hematite (α-Fe2O3). Hematite is the oldest known of the iron oxides and is widespread in rocks and soils. It is also known as ferric oxide, iron sesquioxide, red ochre, specularite, specular iron ore, kidney ore, or martite. Hematite is blood-red in color if finely divided, and black or grey if coarsely crystalline. It is extremely stable at ambient conditions, and often is the end product of the transformation of other iron oxides. Magnetite is also known as black iron oxide, magnetic iron ore, loadstone, ferrous ferrite, or Hercules stone. It exhibits the strongest magnetism of any transition metal oxide. Maghemite occurs in soils as a weathering product of magnetite, or as a product of heating of other iron oxides. It is metastable with respect to hematite, and forms continuous solid solutions with magnetite.
The important features of Hematite (α-Fe2O3) is its density (5.312 gm/cc), and it is weakly ferromagnetic or antiferromagnetic, melting point is about 1350 °C, and the crystallographic system is rhombohedral or hexagonal. By modifying the growth conditions, the size of the iron oxide particles can be reduced to nanosize. The crystal structure of the technologically important Hematite is shown in Fig. 1.

• *AKIBA FEXY J D H, M.E. (APPLIED ELECTRONICS), Loyola Institute of Technology and Science, Loyola Nagar, Thovalai, Kanyakumari District, India. Email-ID: akibafexy@gmail.com*

The iron atom has a strong magnetic moment due to four unpaired electrons in its 3d orbitals. When crystals are formed from iron atoms, different magnetic states can arise. In the paramagnetic state, the individual atomic magnetic moments are randomly aligned with respect to each other, and the crystal has a zero net magnetic moment. If this crystal is subjected to an external magnetic field, some of these moments will align, and the crystal will attain a small net magnetic moment. In a ferromagnetic crystal, all the individual moments are aligned even without an external field. A

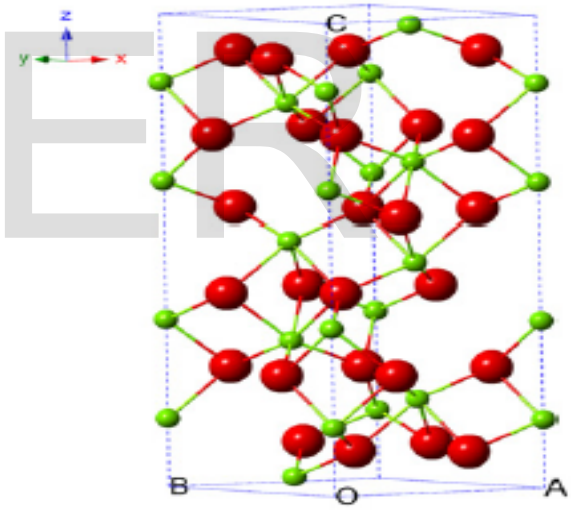

Fig. 1 Crystal structure and crystallographic data of hematite (green ball is Fe3+ and the red ball is O2-)

ferromagnetic crystal, on the other hand, has a net magnetic moment from two types of atoms with moments of different strengths that are arranged in an antiparallel fashion. If the antiparallel magnetic moments are of the same magnitude, then the crystal is antiferromagnetic and possesses no net magnetic moment. Hematite is paramagnetic at temperatures above its Curie temperature of 956 K. At room temperature, it is weakly ferromagnetic and undergoes a phase transition at 260 K (the Morin temperature, TM) to an antiferromagnetic. The magnetic behavior of hematite depends on crystallinity, particle size and on the extent of cation substitution. The Morin temperature of hematite decreases as the particle size decreases and tends to vanish for particles smaller than 8 - 20

nm. Poor crystallinity and substitution of cations tend to lower TC and TM (and may even completely suppress the Morin transition) at all temperatures.

Since iron oxide is a technology important material, a systematic study has been initiated to prepare it through sol-gel method using ferric chloride as the precursor and ammonium hydroxide as the reducing agent. Prepared nanoparticles have been analyzed to evaluate its structural properties from X-ray diffraction studies. Structural parameters such as lattice parameter, unit cell volume, density, crystalline size, micro strain, dislocation density, texture co-efficient were all extracted from the XRD data.

2 Experimental

Iron oxide nanoparticles were synthesized using sol-gel method. In sol-gel method, there are two types of materials or components, "sol" and "gel". Sols are solid particles in a liquid subclass of colloids and gels are ligands contained in liquid. This method can produce highly pure and well controlled nanoparticle. It is a low temperature, less energy consumption and less pollution process. This process involves formation of sols in a liquid and it is reduced to the desired product using a reducing agent. In the present study Ferric Chloride is used as the precursor, Ethanol as the solvent and Ammonium Hydroxide as the reducing agent. Initially, Ferric Chloride is dissolved in the solvent and the reducing agent is added drop by drop to produce the iron oxide nanoparticles. The Ethanol and Ammonium Hydroxide is added in 4:1 radio for a makeup of 0.5M (200ml) solution. Prepared sample is then washed repeatedly using water and ethanol in-order to remove the impurities. Then they were dried to get the Nano powder. The yield was about 19.520gms. Then half of the sample was calcinated at 300°C for 3hrs. and the sample is hence forth mentioned as FeO-1 and the remaining half was calcinated at 800°C for 3hrs. and is named as FeO-2.

3 Results And Discussion

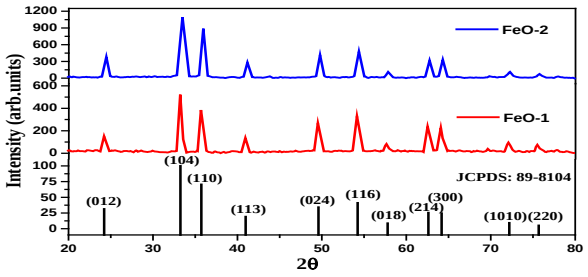

Fig. 2 X-Ray spectra of the synthesized iron oxide nanoparticles.

Fig. 2 shows the X-ray diffraction spectra of the synthesized iron oxide nanoparticles (FeO-1 & FeO-2).

The synthesized iron oxide nanopowders were characterized using X-ray diffraction. XRD pattern indicates that the prepared iron oxide was in α-Fe2O3 phase exhibiting rhombohedral structure. Observed peaks are in defined positions that shows the formation of α-Fe2O3 without any impurity peaks of any other phase of iron oxide, which indicates a high degree of purity of the prepared samples. The broadening of the X-ray diffraction lines reflects the nanoparticle nature of the sample. In XRD, all the peaks are indexed and the d-values are compared with the JCPDS standards [JCPDS file no. 89-8104]. Using the XRD data all other related structural parameters have been calculated.

The unit cell edges was calculated using the equation:

$$\frac{1}{d^2} = \frac{4}{3}\left(\frac{h^2+hk+k^2}{a^2}\right) + \frac{l^2}{c^2}$$

where, 'd' is the inter planner distance, 'a', 'c' are the lattice parameters and 'h, k, l' are the Miller indices of lattice planes. The unit cell volume was calculated using the equation;

$$unit\ cell\ volume, V = \frac{\sqrt{3}\,a^2\ c}{2}\ (Å^3)$$

where 'a','c' are the lattice parameters.

The density was calculated using;

$$Density, \rho = \frac{FW * Z * 1.66}{Unit\ cell\ volume}\ (gm/cc^3)$$

where, 'FW' is the formula weight which is 159.69 for Fe2O3

Z = 6 (No. of units of Fe2O3 in a unit cell)

The crystalline size was calculated using:

$$D = \frac{0.97 * \lambda}{\beta_{2\theta} * cos\theta}\ (nm)$$

where; λ = 1.5462 Å, β2θ = FWHM in radian

The micro strain was calculated using:

$$\varepsilon = \frac{\beta_{2\theta} * cos\theta}{4}$$

where; β2θ = FWHM in radian

The dislocation density was calculated using:

$$\delta = \frac{1}{D^2}\ (lines/m^2)$$

where; D is the crystalline size

The texture co-efficient was calculated using:

$$TC = \frac{{}^{I_{hkl}}/_{I_{O_{hkl}}}}{{}^{1}/_{N} * \sum_{N} {}^{I_{hkl}}/_{I_{O_{hkl}}}}$$

where; 'I' is the intensity and 'N' is the total number of peaks.

TABLE I. LATTICE PARAMETER OF THE PREPARED A-FE2O3 NANOPARTICLE

SAMPLE DETAILS	LATTICE PARAMETER (Å)		UNIT CELL VOLUME (Å3)	
	EXPERIMENTAL	STANDARD	EXPERIMENTAL	STANDARD
FEO-1	A = 4.99500 C=13.62666	A = 5.023 C=13.708	294.436086	299.52
FEO-2	A = 5.03170 C=13.73443		301.14159	

In FeO-1 the lattice parameter value is less compared to the standard lattice parameter, this is because of the preparative parameters. As the sample FeO-1 was prepared at low temperature, many of the lattice sites are vacant. Hence the lattice length both in 'a' and 'c'-axis is less compared to the standard bulk sample. However, in FeO-2, the sample calcined at 800°C, all the lattice sites are completely filled and hence the lattice parameter value is nearly equal to the standard lattice parameter value. Since the lattice parameter is less in FeO-1, the unit cell volume is less compared to the standard unit cell volume. Since every lattice locations are filled with Fe and O ions in FeO-2, the unit cell volume is increased and it is nearly equal to the standard unit cell volume.

TABLE II. RELATED STRUCTURAL PARAMETER OF A-FE2O3 NANOPARTICLE

SAMPLE DETAILS	DENSITY (GM/CC3)		CRYSTALLINE SIZE (D) NM	MICRO STRAIN	DISLOCATION DENSITY (*10^15) LINES/M2
	EXP.	STANDARD			
FEO-1	5.40189	5.312	22.71590	0.00162	1.93793
FEO-2	5.281609		24.17427	0.00152	1.7117

As the volume decreases, the density increases and vice versa. Hence as the unit cell volume of FeO-1 is less the density value is increased and it is high compared to its standard density value. Since the unit cell volume of FeO-2 is high or nearly equal to the standard value the density value is reduced and it is less than the standard density value. As the temperature increases, the particle size increases. Here FeO-1 which is calcinated at 300°C has the crystalline size of about 22 nm and as the calcination temperature is increases to about 800°C for FeO-2, the crystallite size increases to 24 nm. Hence as the temperature increases the crystalline size also increases. Crystalline size and micro strain are interrelated and so the micro strain value of FeO-1 is high compared to FeO-2. Since microstrain and the defect parameter, dislocation density are correlated, the FeO-1 has more defects.

TABLE III. TEXTURE CO-EFFICIENT OF FEO-1

INTENSITY		HKL	TC
OBSERVED	STANDARD		
34.7	313	0 1 2	0.9536
100	999	1 0 4	0.86102
81.4	704	1 1 0	0.99456
25.5	190	1 1 3	1.15443
37.8	341	0 2 4	0.95349
43.6	410	1 1 6	0.91471
10.2	85	0 1 8	1.03219
28.9	254	2 1 4	0.97869
30.1	245	3 0 0	1.05677
10.2	92	1 0 10	0.95366
6.8	51	2 2 0	1.14688

The preferential orientation of the films can be studied by calculating the texture coefficient TC(hkl) for all the planes. The variation in the texture co-efficient has been calculated for all the diffraction peaks i.e. the (0 1 2), (1 0 4), (1 1 0), (1 1 3), (0 2 4), (1 1 6), (0 1 8), (2 1 4), (3 0 0), (1 0 10) and (2 2 0). It is observed that the (1 1 3) plane has a high texture co-efficient of 1.15443. Hence the crystalline growth is mostly oriented in (1 1 3) direction.

The variation in the texture co-efficient has been calculated for all the diffraction peaks of FeO-2 sample i.e. the (0 1 2), (1

0 4), (1 1 0), (1 1 3), (0 2 4), (1 1 6), (0 1 8), (2 1 4), (3 0 0), (1 0 10) and (2 2 0). It is observed that the (2 2 0) plane has a high texture co-efficient of 1.76864.

TABLE IV. TEXTURE CO-EFFICIENT OF FEO-2

INTENSITY		HKL	TC
OBSERVED	STANDARD		
28.8	313	0 1 2	0.57636
100	999	1 0 4	0.62702
73.7	704	1 1 0	0.65576
26	190	1 1 3	0.85717
51.3	341	0 2 4	0.94235
63.1	410	1 1 6	0.96404
15.6	85	0 1 8	1.14962
45.4	254	2 1 4	1.11962
43.3	245	3 0 0	1.10706
18.1	92	1 0 10	1.23236
14.4	51	2 2 0	1.76864

4 CONCLUSION

The iron oxide nanoparticle with hematite phase was prepared using sol-gel process. Structural parameters were evaluated from the X-ray diffraction studies. From the evaluated structural parameters, the α-Fe2O3 nanoparticles prepared after calcination to a temperature of 800°C exhibited perfect lattice with less strain values.

REFERENCES

[1] Ling Li, Maohong Fan, Robert C. Brown, and J. (Hans) Van Leeuwen; Synthesis, Properties, and Environmental Applications of nanoscale Iron-Based Materials: A Review (2006).

[2] Wei Wu, Zhaohui Wu, Taekyung Yu, Changzhong Jiang and Woo-Wik Kim; Recent progress on magnetic iron oxide nanoparticles: synthesis, surface functional strategies and biomedical applications (2015).

[3] Hasany. S.F, Ahmed.I, Rajan.J, Rehman.A; Systematic Review of the Preparation Techniques of Iron Oxide Magnetic Nanoparticles (2012).

[4] Eunice Aparecida Campos, Denise Villela Barcza Stockler Pinto, Jose Irineu Sampaio de Diveira, Elizabeth da Costa Mattos, Rita de Cassia Lazzarini Dutra; Synthesis, Characterization and Applications of Iron Oxide Nanoparticles – a Short Review.

[5] Aleksandr Marinin; Synthesis and characterization of superparamagnetic iron oxide nanoparticles coated with silica (2012).

[6] Amyn S. Teja, Pei-Yoong Koh; Synthesis, properties and applications fo magnetic iron oxide nanoparticles (2009).

[7] Joan Estelrich, Maria Jesus Saanchez-Martin, Maria Antonia Busquets; Nanoparticles in magnetic resonance imaging: from simple to dual contrast agents (2015).

[8] Mohapatra .M and Anand.S; Synthesis and applications of nano-sturctured iron oxides/hydroxides – a review (2010).

[9] Marcos Fernandez-Garcia, Jose A. Rodriguez; Metal Oxide Nanoparticles (2007).

[10] Nohyun Lee and Taeghwan Hyeon; Designed synthesis of uniformly sized iron oxide nanoparticles for efficient magnetic resonance imaging contrast agents (2011).

[11] Ulrich. I. Tromsdorf, Oliver T.Bruns, Sunhild C.Salmen, Ulrike Beisiegel, and Horst Weller; A Highy Effective, Nontoxic T1 MR Contrast Agent Based on Ultrasmall PEGylated Iron Oxide Nanoparticles (2009).

[12] Ja Young Park, Myung Ju Baek, Eun Sook Choi, Seungtae Woo, Joo Hyun Kim, Tae Jeong Kim, Jae Chang Jung, Kwon Seok Chae, Yongmin Chang, and Gang Ho Lee; Paramagnetic Ultrasmall Gadolinium Oxide Nanoparticles as Advanced T1 MRI Contrast Agent: Account for Large Longitudinal Relaxivity, Optimal Particle Diameter, and In Vivo T1 MR Images (2009).

[13] Neuwelt .E.A, Varallyay.P, Bago. A.G, Muldoon L.L, Nesbit.G, and Nixon.R; Imaging of iron oxide nanoparticles by MR and light microscopy in patients with malignant brain tumours (2004).

[14] Hyon Bin Na, Jung Hee Lee, Kwangjin An, Yong II Park, Mihyun Park, In Su Lee, Bo-Hyun Nam, Sung Tae Kim, Seung-Hoon Kim, Keun-Ho Lim, Ki-Soo Kim, Sun-Ok Kim, and Taeghwan Hyeon; Development of a T1 Contrast Agent for Magnetic Resonance Imaging Using MnO Nanoparticles.

[15] Stephane Roux, Anne-Charlotte Faure, Celine Mandon, Sandrine Dufort, Charlotte Riviere, Jean-Luc Bridot, Brice Mutelet, Christophe A Marquette, Veronique Josserand, Geraldine Le Duc, Alain Le Pape, Claire Billotey, Marc Janier, Jean-Luc Coll, Pascal Perriat and Olivier Tillement; Multifunctional gadolinium oxide nanoparticles: towards image-guided therapy.

[16] Anna Moore, Edgardo Marecos, Alexei Bogdanov, Ralph Weissleder; Tumoral Distribution of Long-circulating Dextran-coated Iron Oxide Nanoparticles in a Rodent Model.

[17] Ajay Kumar Gupta, Rohan R Naregalkar, Vikas Deep Vaidya and Mona Gupta; Recent advances on surface engineering of magnetic iron oxide nanoparticles and their biomedical applications.

[18] Shakeel Akbar, Hasanain S.K., Nasia Azmar and Nadeem .M, Synthesis of Fe2O3 nanoparticles by new Sol-Gel method and their structural and magnetic characterizations.

[19] Suender Duhan and Sunita Devi; Synthesis and Structural Characterization of Iron Oxide Nanocomposites Prepared by the Solgel method (2010).

[20] Kulkarni S.A, Sawadha P.S, Kokate K.K; Sunthesis and Characterization of Fe3O4 Nanoparticles for Engineering Applications (2012).

[21] Tharani K., Nehru L.C., Synthesis and Characterization of Iron Oxide Nanoparticles by Precipitation Method.

[22] Sara Shaker, Shirzad Zafarian, Shilpa Chakra C.H., Venkateswara RaoK., Preparation and characterization of magnetite nanoparticles by sol-gel method for water treatment (2013).

[23] Santimukul Santra, Charalambos Kaittanis, Jan Grimm and Manuel Perez J., Drug/Dye-Loaded, Multifunctional Iron Oxide Nanooparticles for Combined Targeted Cancer Therapy and Dual Optical/Magnetic Resonance Imaging.

[24] Andrade A.L, Souza D.M, Pereira M.C, Fabris J.D, Domingues R.Z, Synthesis and characterization fo magnetic nanoparticles coated silica through a sol-gel approach (2009).

[25] Syed Farhan Hasany; Synthesis, Characterization and optimization of magnetic nanostructures by sol-gel technique and application in water purification (2014).

[26] Arturo I. Martinez, Garcia-Lobato M.A, and Dale L. Perry; Study of the properties of iron oxide nanostructures (2009).

[27] Andrew Z. Wang, Vaishali Bagalkot, Christophoros C. Vasilliou, Frank Gu, Frank Alexis, Liangfang Zhang, Mariam Shaikh, Kai Yuet, Michael J. Cima, Robert Langer, Philip W. Kantoff, Neil H. Bander, Sangyong Jon, and Omid C. Farokhzad; Superparamagnetic Iron Oxide Nanoparticle – Aptamer Bioconjugates for Combined Prostate Cancer Imaging and Therapy.

[28] Aurelija Gatelyte, Darius Jasaitis, Aldona Beganskiene, Aivaras Kareiva; Sol-Gel Synthesis and Characterization of Selected Transition Metal Nano-

Ferrites (2011).

[29] Wei Wu, Quanguo He, Changzhong Jiang; Magnetic Iron Oxide Nanoparticles: Synthesis and Surface Functionalization Strategies (2008).

[30] Manasmita Das, Debasish Mishra, Prasanta Dhak, Satyaijit Gupta, Tapas Kumar Maiti, Amit Basak, and Panchanan Pramanik; Biofuntionalized, Phosphonate-Grafted, Ultrasmall Iron Oxide Nanoparticles for Combined Targeted Cancer Therapy and Multimodal Imaging (2009).

[31] Mi Kyung Yu, Dongkyu Kim, In-Hyun Lee, Jee-Soo So, Yong Yeon Jeong, and Sangyong Jon; Image –Guided Prostate Cancer Therapy Using Aptamer-Functionalized Thermally Cross-Linked Superparamagnetic Iron Oxide Nanoparticles (2011).

[32] Hongtao Cui, Marcos Zayat and David Levy; Sol-Gel Synthesis of Nanoscaled Spinels Using Propylene Oxide as a Gelation Agent (2005).

[33] Wei Wu, Quanguo He, Changzhong Jiang; Magnetic Iron Oxide Nanoparticles: Synthesis and Surface Functionalization Strategies (2008).

[34] Swee Kuan Yen, Parasuraman Padmanabhan and Subramanian Tamil Selvan; Multifunctional Iron Oxide Nanoparticles for Diagnostics, Therapy and Macromolecule Delivery.

[35] Ajay Kumar Gupta, Mona Gupta; Synthesis and surface engineering of iron oxide nanoparticles for biomedical applications (2004).

[36] Sophie Laurent, Delphine Forge, Marc Port, Alain Roch, Caroline Robic, Luce Vander Elst and Robert N. Muller; Magnetic Iron Oxide Nanoparticles:Synthesis, Stabilization, Vectorization, Physicochemical Characterization, and Biological Appliations (2008).

[37] Swadeshmukul Santra, Rovelyn Tapec, Nikoleta Theodoropoulou, Jon Dobson,Arthur Hebard, and Weihong Tan; Synthesis and Characterization of Silica-Coated Iron Oxide Nanoparticles in Microemulsion: The Effect of Nonionic Surfactants (2001).

[38] Kyoungja Woo, Jangwon Hong, Sungmoon Choi, Hae-Weon Lee, Jae-Pyong Ahn, Chul Sung Kim and Sang Won Lee; Easy Synthesis and Magnetic Properties of Iron Oxide Nanoparticles (2004).

[39] Daniel J. Korchinski, May Taha, Runze Yang, Nabeela Nathoo and Jeff.F. Dunn; Iron Oxide as an MRI Contrast Agent for Cell Tracking (2015).

[40] Fengqin Hu, Qiaojuan Jia, Yilin Li and Mingyuan Gao; Facile synthesis fo ultrasmall PEGylated iron oxide nanoparticles for dual-contrast T1 and T2 Weighted magnetic resonance imaging (2011).

[41] Dmitri Artemov, Noriko Mori, Baasil Okollie, and Zaver M. Bhujwalla; MR Molecular Imaging of the Her-2/neu Receptor in Breast Cancer Cells Using Targeted Iron Oxide Nanoparticles (2003).

[42] Jean-Luc Bridot, Anne-Charlotte Faure, Sophie Laurent, Charlotte Riviere, Claire Billotey, Bassem Hiba, Marc Janier, Veronique Josserand, Jean-Luc Coll, Luce Vander Elst, Robert Muller, Stephane Roux, Pascal Perriat, and Olivier Tillement; Hybrid Gadolinium Oxide Nanoparticles: Multimodal Contrast Agents for in Vivo Imaging (2007).

[43] Costas G. Hadjipanayis, Michael J. Bonder, Srinivasan Balakrishnan, Xiaoxia Wang, Hui Mao, and George C. Hadjipanayis; Metallic Iron Nanoparticles for MRI contrast enhancement and Local Hyperthermia (2008).

[44] Ali Yadollahpour, Seyed Ahmad Hosseini, Samaneh Rashidi and Fariba Farhadi; Applications of Magnetic Nanoparticles as Contrast Agents in MRI: Recent Advances and Clinical Challenges.

[45] Dongkyu Kim, Sangjin Park, Jae Hyuk Lee, Yong Yeon Jeong,, and Sangyong Jon; Antibiofouling Polymer-Coated Gold Nanoparticles as a Contrast Agent for in Vivo X-ray Computed Tomography Imaging (2007).

[46] Tapan K. Jain, Marco A. Morales, Sanjeeb K. Sahoo, Diandra L. Leslie-Pelecky, and Vinod Labhasetwar; Iron Oxide nanoparticles for Sustained Delivery of Anticancer Agent (2005).

[47] Haerim Lee, Eunhye Lee, Do Kyung Kim, Nam Kyu Jang, Yong Yeon Jeong, and Sangyon Jon; Antibiofouling Polymer-Coated Superparamagnetic Iron Oxide Nanoparticles as Potential Magnetic Resonance Contrast Agents for in Vivo Cancer Imaging (2006).

[48] Haerim Lee, Mi Kyung Yu, Sangjin Park, Sungmin Moon, Jung Jun Min, Yong Yeon Jeong, Hae-Won Kang and Sangyong Jon; Thermally Cross-Linked Superparamagnetic Iron Oxide Nanoparticles: Synthesis and Application as Dual Imaging Probe for Cancer in Vivo (2007).

[49] Carlos Tassa, Stanley Y. Shaw and Ralph Weissleder; Dextran- Coated Iron Oxide Nanoparticles: A Versatile Platform for Targeted Molecular Imaging, Molecular Diagnostics, and Therapy (2011).

[50] Ye Cong, Jinlong Zhang, Feng Chen, Masakazu Anpo and Dannong He; Prepartion, Photocatalytic Activity, and Mechanism of Nano-TiO2-Co-Doped with Nitrogen and Iron(III) (2007).

[51] Brinda B.Lakshmi, Charles J.Patrissi, and Charles R.Martin; Sol-Gel Template Synthesis fo Semiconductor Oxide Micro- and Nanostructures (1997).

[52] Brian L.Cushing, Vladimir L.Kolesnichenko and Charles J.O.Connor; Recent Advances in the Liquid-Phase Synthesis of Inorganic Nanoparticles (2004).

[53] Sun Sheng-Nan, Wei Chao, Zhu Zan-Zan, Hou Yang-Long, Subbu S.Venkatraman, and Xu Zhi-Chuan; Magnetic iron oxide nanoparticles: Synthesis and surface coating techniques for biomedical applications (2014).

[54] Hoon Choi, Seok Rye Choi, Rong Zhou, Hank F.Kung, I-Wei Chen; Iron Oxide Nanoparticles as Magnetic Resonance Contrast Agent for Tumor Imaging via Folate Receptor-targeted Delivery (2004).

[55] Jeff W.M.Bulte, and Dara L.Kraitchman; Iron oxide MR contrast agent for molecular and cellular imaging (2004).

[56] Scott Enochs .W, Griffith Harsh, Fred Hochberg and Ralph Weissleder; Improved Delineation fo Human Brain Tumors on MR Images Using a Long-Circulating, Superparamagnetic Iron Oxide Agent.

[57] Neuwelt E.A, Varalllyay .P, Bago A.G, Muldoon L.L,Nesbit .G, and Nixon R.; Imaging of iron oxide annoparticles by MR and light microscopy in patients with malignant brain tumours (2004).

[58] Wei Li, Sean Tutton, Anthony T.Vu, Linda Pierchala, Belinda S.Y. Li, Jerome MM.Lewis, Pottumarthi V.Prasad, and Robert R. Edelman; First-Pass Contrast-Enhanced Magnetic Resonance Angiography in Humans Using Ferumozytol, a Novel Ultrasmall Superparamagnetic Iron Oxide (USPIO)-Based Blood Pool Agent (2005).

[59] Joseph T.Ferrucci and David D.Stark; Iron Oxide-Enhanced MR Imaging of the Liver and Spleen: Review of the first 5 Years (1990).

[60] Conroy Sun, Chen Fang, Zachary Stephen, Omid Veiseh, Stacey Hansen, Donghoon Lee, Richard G Ellenbogen, Jim Olson, and Miqin Zhang; Tumor-targeted drug delivery and MRI contrast enhancement by chlorotoxin-conjugated iron oxide nanoparticles.

[61] Costas G. Hadjipanayis, Michael J.Bonder, Srinivasan Balkrishnan, Xiaoxia Wang,Hui Mao, and George C.Hadjipanayis; Metallic Iron Nanoparticles for MRI contrast Enhancement and Local Hypertermia (2008).

[62] Amyn S.Teja, Pei-Yoong Koh; Synthesis, properties, and applications of magnetic iron oxide nanoparticles (2009).